New Dithiolate-bridged Rhodium Complexes†

Anna M. Masdeu,[a] Aurora Ruiz,[a] Sergio Castillón,[a] Carmen Claver,[a] Peter B. Hitchcock,[b] Penny A. Chaloner,[b] Carles Bó,[a] Josep M. Poblet[a] and Pedro Sarasa[c]

[a] *Departament de Química, Facultat de Química, Universitat Rovira i Virgili, Pl. Imperial Tarraco 1, 43005 Tarragona, Spain*

[b] *School of Chemistry and Molecular Sciences, University of Sussex, Falmer, Brighton BN1 9QJ, UK*

[c] *Departamento de Química Orgánica y Química Fisica, Universidad de Zaragoza, Pz. San Francisco s/n, 50009 Zaragoza, Spain*

Addition of a dithiol ligand $HS(CH_2)_nSH$ (n = 2–4) to $[\{Rh(\mu\text{-}OMe)(cod)\}_2]$ (cod = cycloocta-1,5-diene) afforded dithiolate-bridged complexes $[\{Rh_2[\mu\text{-}S(CH_2)_nS](cod)_2\}_x]$ (x = 1 or 2). These diene complexes react with carbon monoxide to give the binuclear tetracarbonyl complexes $[Rh_2\{\mu\text{-}S(CH_2)_nS\}(CO)_4]$. The crystal structures of $[Rh_2\{\mu\text{-}S(CH_2)_nS\}(cod)_2]$ (n = 2 or 3) have been determined by X-ray diffraction methods. A study of the electronic structure of the complexes by analysis of the topology of the charge density shows that in spite of a zero formal bond order between the rhodium atoms a direct metal–metal interaction may be characterized.

Thiolate-bridged dirhodium complexes have been extensively investigated[1–16] because of their catalytic activity in hydroformylation reactions under mild conditions.[13,16–20] X-Ray structural studies on some selected thiolate,[10–13] fluorothiolate[14–16] and aminothiolate[19] complexes have shown that they exist as 'bent' double square-planar structures.

An advantage of using these new types of dinuclear complexes is that they allow the possibility of introducing subtle changes in the bridging ligands. Varying the substitution in the thiolate ligands may improve the properties of the complexes as catalyst precursors and should give some information as to the influence of the substituents on the catalytic process. Furthermore, choice of appropriate ligands in some cases allows the recovery of the costly rhodium complex at the end of the hydroformylation reaction, and it can then be reused without loss of reactivity.[20]

However, dithiolate-bridged rhodium complexes have been little studied. Continuing our studies of dinuclear rhodium complexes, we considered it interesting to prepare, characterize and study some new dinuclear rhodium dithiolate-bridged complexes, which may give rise to different structures. Owing to the short Rh–Rh distances measured in the dinuclear thiolate complexes described, which are shorter than in related thiolate-bridged complexes in which it had been concluded that there were metal–metal interactions,[11–14] it was considered of interest to study the electronic structure of these complexes in order to investigate the possible existence of a metal–metal interaction. A new way of defining atoms in molecules and their interactions with respect to the distribution of the charge density ρ has been developed by Bader *et al.*[21,22] The properties of the electronic charge density are investigated through the analysis of its associated fields. A connection has been established between the structure of a molecular system and the gradient vector field, $\nabla\rho$, introducing the concept of bond path. A bond path is defined as the line linking two nuclei along which the charge density corresponds to a maximum with respect to any neighbouring line. According to Bader,[21] the presence of a bond path at the equilibrium geometry represents a necessary and sufficient condition for the existence of a bond. It has furthermore been shown that the Laplacian of $\rho(r)$ identifies regions wherein the electronic charge is either locally concentrated or depleted.[22b] Concentrations of charge appear in both the bonded and non-bonded regions of an atom, and can be correlated with the Lewis electron pairs, for which they provide a physical interpretation.[23]

* *Supplementary data available:* see Instructions for Authors, *J. Chem. Soc., Dalton Trans.*, 1993, Issue 1, pp. xxiii–xxviii.

Non-SI unit employed: cal = 4.184 J.

Theoretical

The wavefunctions were computed at the linear combination of atomic orbitals–molecular orbital–self-consistent field (LCAO–MO–SCF) level by using a CRAY version of the ASTERIX system of programs.[24] The complex $[Rh_2\{\mu\text{-}S(CH_2)_2S\}(cod)_2]$ (cod = cycloocta-1,5-diene) was modelled to the C_{2v} point group and the cod ligands were replaced by two C_2H_4 groups with the same spatial distribution as the cods in the complex. The Gaussian basis set for rhodium was taken from the 15s, 9p, 8d set of Veillard and Dedieu,[25] incremented with an extra p function of exponent 0.15, and contracted to [6,4,4]). For sulfur a 11s, 7p basis set from Huzinaga[26] contracted to [4,3] was employed. For carbon and hydrogen atoms, 9s, 5p and 4s basis sets respectively were used, and contracted to [3,2] and [2].[26]

The topology of the charge density of $[Rh_2(\mu\text{-}SCH_2CH_2S)(cod)_2]$ was studied in order to determine whether charge is locally concentrated or depleted; this analysis uses the gradient and the laplacian of the charge density. The first derivatives of ρ vanish at a critical point (r_c). The second derivatives of ρ determine the three curvatures of ρ at r_c. A critical point is then characterized by its rank, the number of non-vanishing curvatures of ρ, and its signature, the algebraic sum of signs of the curvatures. For critical points of rank 3, four values of the signature are possible: −3, −1, +1, +3. A (3, −3) critical point denotes a local maximum in $\rho(r)$, while a (3, +3) critical point is a local minimum. The other two critical points are associated with saddle points in the charge-density distribution. At the atomic nuclei the charge density displays a local maximum. A (3, +3) cage critical point exists at the point of minimum charge density inside a cage of atoms, whereas a (3, +1) ring critical point appears as a minimum in a ring surface.

A necessary condition for the existence of a bond between two atoms is the presence of a bond path linking both nuclei. The

bond path is the interaction line on which the density is a maximum in all directions perpendicular to this line. On the bond path a (3,−1) bond critical point (b.c.p.) exists. The existence of a bond between the two rhodium atoms should be revealed by topological analysis of the charge density. A b.c.p. between the two metal atoms should be observed if the bond exists. Such points were found between the rhodium atoms in $[Rh_2\{NC(S)(CH_2)_3\}_4(CO)]$, and between the vanadium atoms in $[V_2(\mu\text{-}\eta^2\text{-}S_2)_2(S_2CH)_4]$, confirming the presence of a single metal–metal bond in both complexes.[27,28] In $[Co_2(CO)_8]$ a b.c.p. was not obtained in the intermetal region at the experimental geometry, but it appeared with a slight shortening of the metal–metal distance.[29]

The value of the charge-density function at a b.c.p. provides a relative indication of the 'bond strength' for a given type of bond; $e = (\lambda_1/\lambda_2) - 1$ represents the ellipticity of the bond, where λ_1 and λ_2 are the negative curvatures of r at the (3,−1) critical point, with $|\lambda_1| < |\lambda_2|$. The ellipticity can be interpreted as giving a relative value of the 'π character'.

The laplacian of ρ ($\nabla^2\rho$) is the sum of three principal curvatures of the charge-density function at each point in space. When $\nabla^2\rho < 0$ the value of ρ at point r is greater than the value of $\rho(r)$ averaged over all neighbouring points in space, and when $\nabla^2\rho(r) > 0$, $\rho(r)$ is less than this averaged value; thus a maximum in $-\nabla^2\rho(r)$ means that electronic charge is locally concentrated in that region, while a minimum in $-\nabla^2\rho(r)$ identifies a local hole in the charge-density distribution. The laplacian of ρ recovers the structure of an atom by displaying a corresponding number of pairs of shells of charge concentration and charge depletion. The spherical valence shell of a free atom is distorted by bond formation; in a molecule the valence shell of charge concentration (v.s.c.c.) of an atom displays 'lumps' and 'holes', analogous to hills and valleys in the description of a surface terrain. The number and positions of the maxima and minima of the laplacian of ρ correspond to the atom's Lewis structure and determine its overall chemical behaviour. The holes are the sites of nucleophilic attack. The local concentrations of charge determine the sites of electrophilic attack. For a more detailed description of the theory of atoms in molecules, see the recent book of Bader.[30]

The topological properties of ρ were calculated with a modified version of the AIMPAC package.[31]

Results and Discussion

Synthesis of Diene and Carbonyl Complexes.—New rhodium dithiolate complexes have been prepared by addition of the corresponding ligand $HS(CH_2)_nSH$ (n = 2–4) to dichloromethane solutions of $[\{Rh(\mu\text{-}OMe)(cod)\}_2]$. In the case of $HS(CH_2)_2SH$ the addition of diethyl ether results in complete precipitation of the complex $[Rh_2\{\mu\text{-}S(CH_2)_2S\}(cod)_2]$ **1**, as a moderately air-stable red solid. This complex had been previously synthesised for comparative purposes, to study alkene rotation in the related complex $[Rh_2(\mu\text{-}SR)_2(cod)_2]$ (R = Me, Et, Pr^i, Bu^t or Ph).[9] The ^{1}H NMR spectrum of this complex shows two signals for each of the alkene (δ 4.3 and 4.6) and methylene (δ 1.9 and 2.1) protons of the co-ordinated cycloocta-1,5-diene, indicating two different environments for each type of protons. This is due to the dinuclear bent structure as was later established in a crystal structure determination. Similarly, the ^{13}C NMR spectrum shows two signals for each of the methylene (δ 31.7 and 31.9) and alkene (δ 80.1 and 80.9) carbons of the co-ordinated cyclooctadiene, indicating two different environments for each type of carbon atom.

Two different products are obtained in the reaction of $[\{Rh(\mu\text{-}OMe)(cod)\}_2]$ with $HS(CH_2)_3SH$. Addition of diethyl ether results in precipitation of a yellow solid, **2**. Concentration and cooling of the remaining solution yielded a red complex, which could be recrystallized and was characterized as $[Rh_2\{\mu\text{-}S(CH_2)_3S\}(cod)_2]$ **3** by a crystal structure determination. Both complexes are insoluble in MeOH, so that addition of MeOH to the initial solution resulted in precipitation of a mixture. Furthermore, although complex **3** gave good microanalytical data, and the structure could be established in the solid state, it was not stable in solution. When **3** was dissolved in $CDCl_3$ to obtain the ^{1}H NMR spectrum, signals due to **2** could be clearly identified. It would appear that **2** is in equilibrium with **3** in solution. The ^{1}H NMR spectrum of a solution of the yellow product shows only a single signal assigned to the alkene protons of the co-ordinated cyclooctadiene ligand (δ 4.1). The ^{1}H NMR spectrum of a solution of the red complex shows, together with the signals corresponding to the alkene (δ 4.3 and 4.6) and methylene protons (δ 2.1 and 2.5) in different environments in the dinuclear complex, another broad signal at δ 4.2 due to the presence of complex **2** in the solution. The integrals ratio (71% complex **3**: 29% complex **2**) shows the distribution of the complexes at equilibrium. There are several signals between δ 2.47 and 1.73 which may be attributed to the CH_2 of the cyclooctadiene and of the co-ordinated ligands, but cannot be specifically assigned. A similar situation is noted for the ^{13}C NMR spectra. The solid-state IR spectra (Nujol) of complexes **2** and **3** are slightly different with respect to the frequencies corresponding to the co-ordinated double bonds and the fingerprint region.

In order to obtain more information about the nuclearity of complex **2** it was examined by FAB mass spectrometry. Although the molecular ion was not observed, there was a peak at m/z = 801, higher than that expected for a dinuclear complex. This suggests that **2** could be a tetranuclear species $[\{Rh_2[\mu\text{-}S(CH_2)_3S](cod)_2\}_2]$. Attempts to obtain a crystal suitable for an X-ray structure determination have been unsuccessful.

The ligand $HS(CH_2)_4SH$ reacts with $[\{Rh(\mu\text{-}OMe)(cod)\}_2]$ to give a yellow product for which the elemental analysis corresponds to the stoichiometry $[\{Rh_2[\mu\text{-}S(CH_2)_4S](cod)_2\}_n]$ **4**. Attempts to obtain a crystal suitable for an X-ray crystal structure determination were unsuccessful. The ^{1}H NMR spectrum **4** shows a broad signal corresponding to the alkene protons of the co-ordinated cyclooctadiene (δ 4.1), together with two signals corresponding to the *endo*- and *exo*-methylenic protons (δ 2.0 and 2.4). As for complex **2**, the FAB mass spectrum showed a peak at m/z = 723, higher than that expected for a dinuclear complex, suggesting that **4** may be a tetranuclear species $[\{Rh_2[\mu\text{-}S(CH_2)_4S](cod)_2\}_2]$.

Bubbling CO through dichloromethane solutions of the diene complexes yields, in all cases, carbonyl complexes formed by displacement of the diene. The elemental analyses of these complexes correspond to the stoichiometry $[Rh_2\{\mu\text{-}S(CH_2)_nS\}(CO)_4]$ (n = 2–4). The Fourier-transform IR spectra of the complexes in CH_2Cl_2 solution show the three stretching frequencies ν(CO) characteristic of tetracarbonyl dinuclear rhodium complexes $[Rh_2\{\mu\text{-}S(CH_2)_nS\}(CO)_4]$ (n = 2 **5**, 3 **6** or 4 **7**).[11–13] Identical IR spectra are obtained from the materials formed on bubbling carbon monoxide through solutions of the complexes **2** and **3** separately or through a mixture of the two. This confirms that **2** and **3** are in equilibrium in solution, and suggests that they may differ only in nuclearity. Although we believe that **4** is tetranuclear, it is clear that dissociation to a dinuclear species must be possible, since **7** is undoubtedly binuclear.

Crystal Structures.—There have been a number of structural studies of dirhodium and diiridium complexes containing bridging thiolate ligands. There have also been many studies of the structurally related species with chloride bridges.[32–38] A related group of complexes is provided by dimers bridged by pyrazole ligands including $[\{M(\mu\text{-}pz)(cod)\}_2]$ (M = Rh or Ir) and $[(tfbb)Rh(\mu\text{-}Cl)\{(\mu\text{-}tz)Rh(CO)_2Cl\}Rh(CO)_2]$ (tfbb = tetrafluorobenzo[5,6]bicyclo[2.2.2]octa-2,5,7-triene, tz = triazolate),[39] *trans*-$[Rh_2(\mu\text{-}pz)_2(CO)_2\{P(OPh)_3\}_2]$[40] and $[Rh_2(\mu\text{-}3,5Me_2\text{-}pz)_2(CS)_2(PPh_3)_2]$ (3,5Me$_2$-pz = 3,5-dimethylpyrazolate).[41] All of these structures are characterized by a bent

Table 1 Fractional atomic coordinates (× 10^4) for $[Rh_2\{\mu\text{-}S(CH_2)_2S\}(cod)_2]$ **1**

Atom	*x*	*y*	*z*
Rh	1093.3(4)	3371.4(1)	1269.8(3)
S(1)	−1660.2(18)	2500	983.7(17)
S(2)	1754.5(21)	2500	−936.3(16)
C(1)	3252(5)	4296(3)	1070(5)
C(2)	4126(6)	3674(3)	2105(6)
C(3)	4561(7)	3719(4)	4010(7)
C(4)	2905(8)	3747(5)	4892(6)
C(5)	879(6)	3682(3)	3820(5)
C(6)	19(5)	4293(3)	2775(5)
C(7)	942(8)	5104(3)	2613(7)
C(8)	2699(8)	5109(3)	1728(3)
C(9)	−2418(10)	2500	−1313(8)
C(10)	−701(11)	2500	−2291(8)

Table 2 Intramolecular distances (Å) and angles (°) with estimated standard deviations (e.s.d.s) in parentheses for $[Rh_2\{\mu\text{-}S(CH_2)_2S\}(cod)_2]$ **1**

Rh–M(1)*	2.027	Rh–M(2)*	2.017
Rh–Rh′	2.876(1)	Rh–S(1)	2.355(1)
Rh–S(2)	2.370(1)	Rh–C(1)	2.152(4)
Rh–C(2)	2.134(4)	Rh–C(5)	2.120(4)
Rh–C(6)	2.142(4)	S(1)–C(9)	1.811(6)
S(2)–C(10)	1.839(7)	C(1)–C(2)	1.387(6)
C(1)–C(8)	1.511(6)	C(2)–C(3)	1.494(7)
C(3)–C(4)	1.434(8)	C(4)–C(5)	1.506(6)
C(5)–C(6)	1.375(6)	C(6)–C(7)	1.496(6)
C(7)–C(8)	1.496(9)	C(9)–C(10)	1.518(11)
M(1)–Rh–M(2)	87.5	S(1)–Rh–S(2)	79.01(4)
M(1)–Rh–S(1)	172.3	M(1)–Rh–S(2)	96.9
M(2)–Rh–S(1)	95.9	M(2)–Rh–S(2)	172.9
Rh–S(1)–C(9)	100.7(2)	Rh–S(2)–C(10)	99.3(2)
Rh–S(1)–Rh′	75.28(4)	Rh–S(2)–Rh′	74.70(4)
C(2)–C(1)–C(8)	124.1(4)	C(1)–C(2)–C(3)	123.8(4)
C(2)–C(3)–C(4)	117.3(4)	C(3)–C(4)–C(5)	117.0(4)
C(4)–C(5)–C(6)	123.3(4)	C(5)–C(6)–C(7)	124.3(4)
C(6)–C(7)–C(8)	115.6(4)	C(1)–C(8)–C(7)	115.3(4)
S(1)–C(9)–C(10)	113.6(4)	S(2)–C(10)–C(9)	114.5(4)
C(3)–C(4)–H(4A)	110(4)	C(3)–C(4)–H(4B)	130(6)
C(5)–C(4)–H(4A)	112(4)	C(5)–C(4)–H(4B)	100(5)
Rh–C(5)–C(6)	72.1(2)	Rh–C(5)–H(5)	105(3)
C(4)–C(5)–C(6)	123.3(4)	C(4)–C(5)–H(5)	117(3)
C(6)–C(5)–H(5)	117(3)	Rh–C(6)–C(5)	70.3(2)
Rh–C(6)–C(7)	113.3(3)	Rh–C(6)–H(6)	107(3)
C(5)–C(6)–C(7)	124.3(4)	C(5)–C(6)–H(6)	119(3)
C(7)–C(6)–H(6)	113(3)	C(6)–C(7)–C(8)	115.6(4)
C(6)–C(7)–H(7A)	105(4)	C(6)–C(7)–H(7B)	104(5)
C(8)–C(7)–H(7A)	105(4)	C(8)–C(7)–H(7B)	118(5)
H(7A)–C(7)–H(7B)	109(6)	C(1)–C(8)–C(7)	115.3(4)
C(1)–C(8)–H(8A)	108(5)	C(1)–C(8)–H(8B)	99(3)
C(7)–C(8)–H(8A)	133(4)	C(7)–C(8)–H(8B)	108(3)
H(8A)–C(8)–H(8B)	81(5)	S(1)–C(9)–C(10)	113.6(4)
S(1)–C(9)–H(9)	101(3)	C(10)–C(9)–H(9)	118(3)
H(9)–C(9)–H(9′)	103(4)	S(2)–C(10)–C(9)	114.5(4)
S(2)–C(10)–H(10)	104(3)	C(9)–C(10)–H(10)	115(4)
H(10)–C(10)–H(10′)	103(5)		

* M(1) and M(2) are the midpoints of the C(1)–C(2) and C(5)–C(6) bonds.

Table 3 Fractional atomic coordinates (× 10^4) for $[Rh_2\{\mu\text{-}S(CH_2)_3S\}(cod)_2]$ **3**

Atom	*x*	*y*	*z*
Rh	1208.2(5)	1650.3(2)	1463.1(4)
S(1)	2090(2)	2500	−600(2)
S(2)	−1448(2)	2500	1403(2)
C(1)	4142(7)	1329(3)	2260(8)
C(2)	3297(8)	762(3)	1183(7)
C(3)	2703(11)	−39(4)	1783(11)
C(4)	939(11)	−64(4)	2507(10)
C(5)	70(8)	734(3)	2830(7)
C(6)	938(8)	1283(4)	3927(7)
C(7)	2897(10)	1162(6)	4993(9)
C(8)	4543(10)	1266(5)	4109(10)
C(9)	98(14)	2500	−2322(11)
C(10)	−1777(15)	2258(6)	−2090(14)
C(11)	−2755(12)	2500	−751(12)

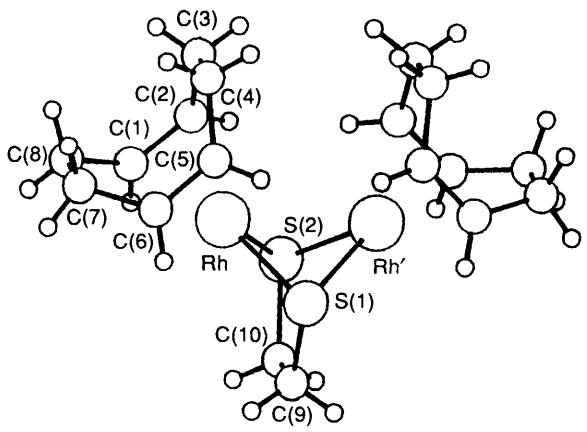

Fig. 1 Spatial diagram of the molecular structure of $[Rh_2\{\mu\text{-}S(CH_2)_2S\}(cod)_2]$

(M_2X_2) ring, with a relatively short metal–metal distance. For previously reported dirhodium dithiolates the rhodium–rhodium distance varies between 2.995 Å for $[\{Rh(\mu\text{-}SC_6F_5)(cod)\}_2]$[14] and 3.391 Å for *cis*-$[Rh_2(\mu\text{-}SCMe_3)(CO)_2\{\mu\text{-}Zr(C_5H_5)_2(CH_2PPh_2)_2\}]$.[12] The angles between the rhodium co-ordination planes range between 113° for *sym-trans*-$[Rh_2(\mu\text{-}SPh)_2(CO)_2(PMe_3)_2]$ and 135° for $[(cod)Rh(\mu\text{-}SPh)_2Rh(CO)_2]$,[9] although it is notable that in some cases the rhodium atoms are displaced slightly from these planes. Complexes of similar gross structure with true Rh–Rh bonds have much shorter metal–metal separations, for example 2.64 Å in $[Rh_2(\mu\text{-}SPh)_2(C_5H_5)_2]$.[42] Separations between two rhodium(III) centres as in $[\{RhCl(H)(\mu\text{-}SH)(PPh_3)_2\}_2]$ (3.737 Å) are generally longer.[43]

The structure of $[Rh_2\{\mu\text{-}S(CH_2)_2S\}(cod)_2]$ **1** consists of discrete dimeric units lying on a crystallographic mirror plane. Atomic coordinates are given in Table 1, and selected bond and distances in Table 2. The structure of dimeric unit is shown in Fig. 1. The rhodium–rhodium distance is 2.876(1) Å, the shortest thus far noted for this type of complex. The angle between the co-ordination planes is particularly acute at 97°, but it is noteworthy that the rhodium atom is displaced by 0.115 Å from the co-ordination plane.

The structure of $[Rh_2\{\mu\text{-}S(CH_2)_3S\}(cod)_2]$ **3** is similar. Atomic coordinates are given in Table 3 and selected bond distances and angles in Table 4. The structure of the dimeric unit is shown in Fig. 2. The rhodium–rhodium distance is also short, at 2.896(1) Å, and the angle between the co-ordination planes 104°, with once more substantial deviation of the rhodium atom from the co-ordination plane (0.13 Å).

These structures represent the first examples of dirhodium dithiolate-bridged complexes to be structurally characterized. It is instructive to compare the available data from the literature (Tables 5–7). From a geometrical point of view three parameters may be used to characterize the metal–metal interactions, *viz.* the metal–metal bond distance, the angle between the co-ordination planes (least-square planes of the four ligands at the metal) and the angle between the planes defined by RhX. These latter two parameters are not in all cases identical, since the rhodium atoms may deviate substantially from the least-squares plane, as indeed they do for the two complexes described here. It is noteworthy that the largest discrepancies between the two

parameters occur when the metal–metal distance is short, generally less than 3 Å, suggesting that the close approach of the metals may be responsible for the distortions. Although there is a general increase in the metal–metal distance as the interplanar angles increase, good linear correlations could not be obtained.

Electronic Structure of $[Rh_2\{\mu\text{-}S(CH_2)_2S\}(cod)_2]$.—The Mulliken population analysis for $[Rh_2\{\mu\text{-}S(CH_2)_2S\}(cod)_2]$ **1** (Table 8) assigns a noticeable charge transfer from the cod ligands and the metal atoms to the $S_2C_2H_4$ fragment. The computed net charges for metal centre, cod ligands and bridging fragment are +0.053, +0.237 and −0.582 e respectively. The electronic structure of the metal atom is characterized by an important population of the 5s + 5p shell (0.671 e). The trend to promote electrons to the outer shell allows the metal centre to increase the bond formation.[44] If *d* electrons only are considered, the electronic structure of **1** agrees with the formal assignment of the metal as Rh^I, d^8.

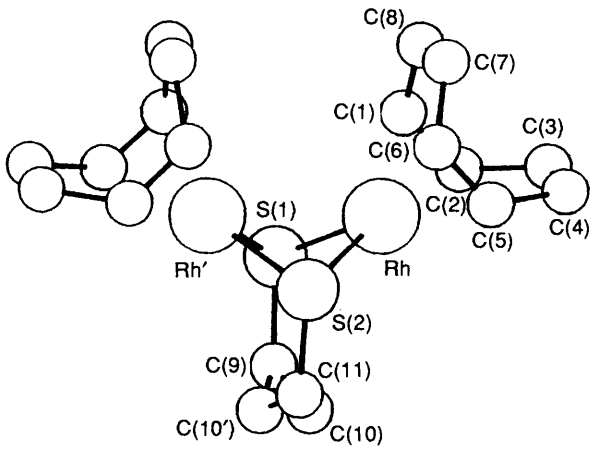

Fig. 2 Spatial diagram of the molecular structure of $[Rh_2\{\mu\text{-}S(CH_2)_3S\}(cod)_2]$

Table 4 Intramolecular distances (Å) and angles (°) with e.s.d.s in parentheses for $[Rh_2\{\mu\text{-}S(CH_2)_3S\}(cod)_2]$ **3**

Rh–M(1)	2.023	Rh–M(2)	2.010
Rh–Rh'	2.896(1)	Rh–S(1)	2.354(2)
Rh–S(2)	2.355(1)	Rh–C(1)	2.127(5)
Rh–C(2)	2.144(6)	Rh–C(5)	2.134(6)
Rh–C(6)	2.108(6)	S(1)–C(9)	1.800(9)
S(2)–C(11)	1.820(9)	C(1)–C(2)	1.366(8)
C(1)–C(8)	1.467(10)	C(2)–C(3)	1.526(9)
C(3)–C(4)	1.449(12)	C(4)–C(5)	1.529(9)
C(5)–C(6)	1.359(8)	C(6)–C(7)	1.512(9)
C(7)–C(8)	1.460(11)	C(9)–C(10)	1.420(14)
C(10)–C(11)	1.424(15)		
M(1)–Rh–M(2)	87.8	M(1)–Rh–S(1)	93.6
M(1)–Rh–S(2)	171.4	M(2)–Rh–S(1)	174.6
M(2)–Rh–S(2)	93.4	S(1)–Rh–S(2)	84.49(5)
Rh–S(1)–Rh'	75.93(6)	Rh–S(1)–C(9)	106.2(3)
Rh–S(2)–C(11)	107.2(2)	Rh–S(2)–Rh'	75.89(5)
C(2)–C(1)–C(8)	125.4(6)	C(1)–C(2)–C(3)	123.1(6)
C(2)–C(3)–C(4)	116.5(6)	C(3)–C(4)–C(5)	115.6(6)
C(4)–C(5)–C(6)	124.9(5)	C(5)–C(6)–C(7)	122.9(6)
C(6)–C(7)–C(8)	115.3(6)	C(1)–C(8)–C(7)	117.4(6)
S(1)–C(9)–C(10)	121.5(7)	C(9)–C(10)–C(11)	125.7(8)
S(2)–C(11)–C(10)	118.9(6)		

A molecular orbital (MO) description of the metal–metal interaction in several bis(pyrazolyl)-bridged iridium dimers, isoelectronic to **1**, has been reported recently.[45] In those dimers the metal–metal bond order is zero[46] and the σ_{M-M} and σ^*_{M-M} orbitals are occupied; however for those complexes Gray and co-workers[45] proposed that there is a substantial interaction between the d_{z^2} atomic orbitals of the two iridium centres.

According to the theory of atoms in molecules, if the electronic structure of $[Rh_2\{\mu\text{-}S(CH_2)_2S\}(cod)_2]$ has a direct metal–metal coupling a bond critical point (b.c.p.) must be found between the two rhodium atoms. In Table 9 are summarized the b.c.p.s determined for **1** at the experimental geometry. Bond critical points have been located between the rhodium atoms and the sulfur atoms, as well as between the metal atoms and the carbon atoms of the diene. Although the cod ligands fill two positions in the co-ordination sphere of the Rh atom, four bonds are determined between the metal centre and the cod ligand.

In the intermetal region no critical points were localized at the experimental geometry. From this result should we conclude that no direct interaction exists between the two metal atoms? In order to analyse this question the geometry effects were studied. Note that in the theory of atoms in molecules a bond critical point is a necessary and sufficient condition for the existence of a bond when the system is in *its equilibrium* geometry. The Rh–Rh and Rh–S distances were optimized by variation of *R* and *r* parameters. In $[Rh_2\{\mu\text{-}S(CH_2)_2S\}(cod)_2]$ small modifications of the Rh–S–Rh angle induced small changes in the energy of the system. If the Rh–Rh distance is

Table 6 Metal–metal distances and interplanar angles in rhodium or iridium μ-chloride complexes

Complex	r_{M-M}/Å	θ[a]/°	φ[b]/°	Ref.
$[\{Ir(\mu\text{-}Cl)(PF_3)_2\}_2]$	2.942	107	95	36
$[\{Rh(\mu\text{-}Cl)(PF_3)_2\}_2]$	2.995	115	105	37
$[\{Rh(\mu\text{-}Cl)(CH_2{=}CHCH{=}CMe_2)_2\}_2]$	3.090	116	105	34
$[\{Rh(\mu\text{-}Cl)(CO)_2\}_2]$	3.12		124	33
$[\{Rh(\mu\text{-}Cl)(CO)(PMe_2Ph)\}_2]$	3.167	125	123	35

[a] Angle between RhS_2 planes. [b] Angle between co-ordination planes.

Table 5 Metal–metal distances and interplanar angles in rhodium or iridium μ-thiolate complexes

Complex	r_{M-M}/Å	θ[a]/°	φ[b]/°	Ref.
$[Rh_2\{\mu\text{-}S(CH_2)_2S\}(cod)_2]$	2.876	104	97	This work
$[Rh_2\{\mu\text{-}S(CH_2)_3S\}(cod)_2]$	2.896	104	112	This work
$[\{Rh(\mu\text{-}SC_6F_5)(cod)\}_2]$	2.955	118	109	14
$[Rh_2\{\mu\text{-}S(CH_2)_3NMe_2\}_2(cod)_2]$	2.960	106	105	19
$[\{Ru(\mu\text{-}SC_6H_4F)(CO)_2\}_2]$[c]	3.076	115	114	16
	3.070	114	111	16
cis-$[\{Rh(\mu\text{-}SPh)(CO)(PMe_3)\}_2]$	3.061	105	107	11
$[(cod)Rh(\mu\text{-}SPh)_2Rh(CO)_2]$	3.12	114	115	9
cis-$[\{Ir(\mu\text{-}SCMe_3)(CO)(PR_3)\}_2]$	3.216	123	122	32
cis-$[Rh_2(\mu\text{-}SCMe_3)(CO)_2\{\mu\text{-}Zr(C_5H_5)_2(CH_2PPh_2)\}_2]$	3.391	137	138	12
$[Rh_2(\mu\text{-}pz)(\mu\text{-}SCMe_3)(CO)_2\{P(OMe)_3\}_2]$	3.447	—	117	13

[a] Angle between RhS_2 planes. [b] Angle between co-ordination planes. [c] Two distinct molecules in the unit cell.

Table 7 Metal–metal distances in rhodium or iridium μ-pyrazolyl complexes

Complex	r_{M-M}/Å	Ref.
$[\{Ir[\mu\text{-}3,5(CF_3)_2\text{-}pz](cod)\}_2]$	3.073	38
$[\{Ir(\mu\text{-}pz)(cod)\}_2]$	3.216	38
$[\{Ir(\mu\text{-}3,5Me_2\text{-}pz)(CO)_2\}_2]$	3.245	38
$[\{Rh(\mu\text{-}pz)(cod)\}_2]$	3.267	38
$[\{Ir(\mu\text{-}pz)(CO)_2\}_2]$	3.502	38
trans-$[Rh_2(\mu\text{-}pz)_2(CO)_2\{P(OPh)_3\}_2]$	3.568	40
$[Rh_2(\mu\text{-}3,5Me_2\text{-}pz)_2(CS)_2(PPh_3)_2]$	3.220	41
$[(tfbb)Rh(\mu\text{-}Cl)\{(\mu\text{-}tz)Rh(CO)_2Cl\}Rh(CO)_2]$*	3.817	39

* The angle between the co-ordination planes is close to 180°.

Table 8 Mulliken population analysis of the wavefunctions computed for $[Rh_2\{\mu\text{-}S(CH_2)_2S\}(cod)_2]$ **1** and $[Rh_2\{\mu\text{-}S(CH_2)_2S\}(CO)_4]$ **5**

Net charges

Complex	Metal	Bridging ligand	cod	CO
1	+0.053	−0.582	+0.237	—
5	+0.211	−0.616	—	+0.048

Atom population

	Total	s	p	d
Rh (**1**)	44.95	8.29	18.38	18.27
(**5**)	44.79	8.29	18.29	18.20
S (**1**)	16.32	5.99	10.34	
(**5**)	16.35	5.98	10.36	
C (**1**)	6.40	3.37	3.03	
(**5**)	6.39	3.40	2.99	
H (**1**)	0.780	0.780		
(**5**)	0.784	0.784		

Table 9 Bond properties in complexes **1**, **5** and **9***

Bond		ρ	$\nabla^2\rho$	Ellipticity
Rh–Rh	(**1**)	—	—	—
	(**5**)	0.031	0.094	1.248
	(**9**)	0.075	0.093	0.912
Rh–S	(**1**)	0.081	0.239	0.227
	(**5**)	0.063	0.194	0.136
	(**9**)	0.056	0.138	0.517
Rh–C(1)	(**1**)	0.091	0.224	0.798
Rh–C(2)	(**1**)	0.094	0.215	0.509
Rh–C	(**5**)	0.113	0.514	0.129
	(**9**)	0.063	0.320	2.564
S–C(9)	(**1**)	0.154	−0.208	0.023
	(**5**)	0.138	−0.142	0.018
	(**9**)	0.064	−0.023	0.254
C(1)–C(2)	(**1**)	0.292	−0.807	0.184
C–O	(**5**)	0.443	0.209	0.001
	(**9**)	0.343	0.358	0.004
C(9)–C(10)	(**1**)	0.232	−0.516	0.021
	(**5**)	0.219	−0.444	0.026
	(**9**)	0.223	−0.488	0.065

* All quantities are in atomic units: for ρ, au = e/a_0^3 = 6.478 e Å^{-3}; for $\nabla^2\rho$, au = e/a_0^5 = 24.10 e Å^{-5}.

increased by 0.2 Å the system becomes destabilized by only 1.7 kcal mol^{-1}. The topological properties of ρ are not altered with the lengthening. If the metal–metal distance is shortened by 0.2 Å the dimer has a relative energy with respect to the experimental geometry of 3.8 kcal mol^{-1}. The shortening of the metal–metal distance induces a change in the topology of the charge density, with a b.c.p. linking the two metal centres. The coupled optimization of *R* and *r* leads to 2.793 and 2.464 Å for the Rh–Rh and Rh–S distances, respectively. The metal–metal distance is slightly shorter than that in the crystal structure, whereas the calculated Rh–S is 0.08 Å longer than the

Table 10 Geometric parameters for the $[Rh_2\{\mu\text{-}S(CH_2)_2S\}(CO)_4]$ and $[Rh_2\{\mu\text{-}S(CH_2)_2S](CO)_4]^{2+}$. Distances in Å, angles in °

	Neutral **5**	Ionic (2+) **8**
Rh–Rh	2.901	2.502
Rh–S	2.484	2.374
S–C	1.886	1.894
C–C	1.545	1.536
Rh–CO	1.989	2.122
C–O	1.134	1.119
Rh–S–Rh	71.4	58.2
S–C–C	116.1	113.9
S–Rh–S	80.3	63.6
H–C–C	110.3	112.0
H–C–H	93.9	107.7
Rh–C–O	175.6	177.9

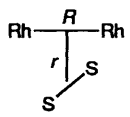

experimental value. The relative energy of the optimized complex is −11.4 kcal mol^{-1}. In the intermetal region a b.c.p. is found between the two rhodium atoms. The electron density at this critical point is 0.035 au. The small value and its elusive character suggests that in $[Rh_2\{\mu\text{-}S(CH_2)_2S\}(cod)_2]$ the direct metal–metal coupling is quite weak. In order to confirm these findings we have carried out calculations on $[Rh_2\{\mu\text{-}S(CH_2)_2S\}(CO)_4]$ **5**; this dinuclear system is detected in solution but it has not yet been determined by X-ray diffraction. The carbonyl ligands are simpler than cod ligands, and a full optimization of the dimer is possible. In this way the condition of the minimum of the potential surface imposed by Bader's theory is accomplished.

Electronic Structure of $[Rh_2\{\mu\text{-}S(CH_2)_2S\}(CO)_4]$.—The computed distances and angles for $[Rh_2\{\mu\text{-}S(CH_2)_2S\}(CO)_4]$ are in Table 10. The geometry has been optimized until the norm of the energy gradient is lower than 1×10^{-3} au. The most significant parameter is the Rh–Rh distance, the value of 2.901 Å being 0.025 Å longer than that experimentally found for **1**. The computed metal–ligand distances are slightly longer than the experimental parameters in similar systems. The calculated Rh–S distance is 2.484 Å, whereas for **1** X-ray diffraction gives a value of 2.370 Å. The rhodium–carbonyl distances also are probably too long. It is established that M–CO interaction is not well described at the SCF level.[47] To reproduce the experimental distances the geometry should be obtained at the configuration interaction (CI) level, and this is outside our present computational abilities. From Table 10 we can see that the other geometric parameters are determined with a reasonable precision. The Mulliken population analysis on carbonyl complex **5** shows that the net charge of the bridging ligand is only slightly higher than in **1**. However, in the carbonyl dimer the transfer of charge arises mainly from the metal centre. The net charge of the rhodium atoms is +0.211e.

Although the computed rhodium–rhodium distance in the carbonyl dimer is longer than experimental distance in **1**, the two metal centres are linked by a bond path. The electron density associated with the bond critical point is 0.031 au. Therefore it must be concluded that the presence of the b.c.p. is not an artefact of the geometry used and that in this kind of dinuclear complex, in spite of a zero formal bond order, a direct coupling exists between the metal centres. The metal–metal interaction must not be considered as a result of a standard rhodium–rhodium bond, since σ_{M-M} and σ^*_{M-M} are occupied orbitals. To emphasize the weak metal–metal coupling, calculations were carried out on $[Rh_2\{\mu\text{-}S(CH_2)_2S\}(CO)_4]^{2+}$ **8**.

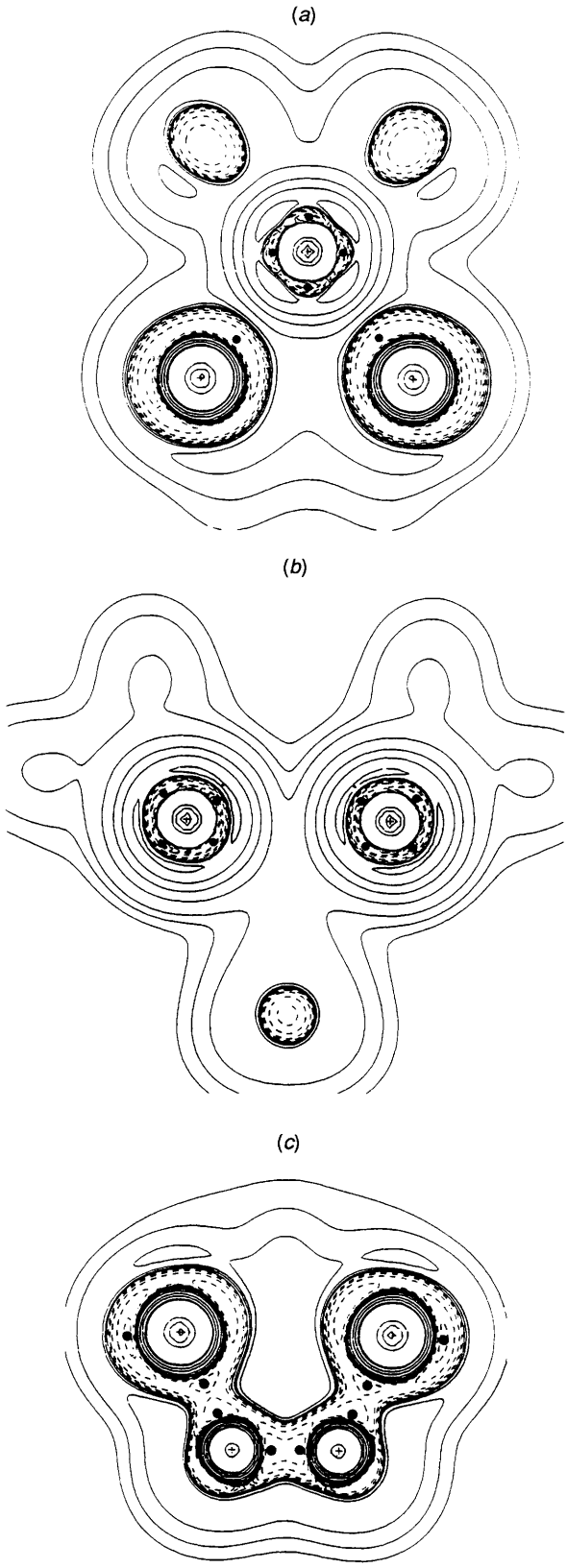

Fig. 3 Contour maps of $\nabla^2\rho$ for planes containing a Rh and two S atoms (*a*), two rhodium centres and the midpoint between the C–C bond of the bridging ligand (*b*) and the SCCS ligand (*c*). Dashed contours are used for negative values of $\nabla^2\rho$, whereas solid lines are for 0 and positive values of the laplacian of ρ. The positions of bonded and non-bonded maxima in the valence shell of charge concentration are indicated by dots. Although in drawing (*a*) two maxima are denoted in the v.s.c.c. of the sulfur atoms, in fact the (3, −3) critical points are slightly displaced from this plane

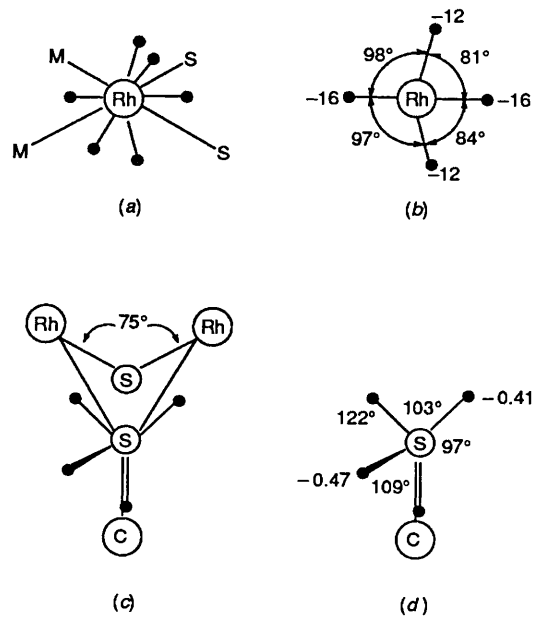

Fig. 4 (*a*) Representation of the six maxima characterized in the i.v.s.c.c. of the Rh atoms. Four of these are in the M_2S_2 plane with values of −16 au (*b*) and two of them are in the perpendicular plane with lower magnitudes (−12 au). These are called axial concentrations in the text. The charge concentrations of the cod ligands exercise a strong repulsion on the axial charges of Rh atoms, which are shifted toward the dithiolate ligand (*b*). The relative positions of the bonded and non-bonded maxima around the sulfur atoms are in (*c*). The angles between the maxima are displayed in (*d*)

The two ionized electrons were removed from the σ^*_{M-M} orbital, so the ionized complex formally should have a single metal–metal bond. A full optimization of the ionized dimer in C_{2v} symmetry led to a minimum of the potential surface. Its geometry represents an important modification of that of the neutral dimer. The calculated parameters are summarized in Table 10. The computed Rh–Rh distance in **8** is 2.502 Å, 0.4 Å shorter than in the neutral complex. The Rh–S distance is also shortened by the oxidation process. On the other hand, the lengthening of the M–CO distance suggests that the formation of a strong metal–metal bond enhances the lability of the carbonyl ligands. If bond distances and density values associated with bond critical points provide relative indications of bond strength, it must be concluded that the ionization of the two electrons of the σ_{M-M}^* orbital reduces the flexibility of the Rh_2S_2 framework of the studied rhodium(I) complexes. In **8** the carbonyls are displaced by 18° from the RhS_2 plane, thus the Rh^{II} is not in a square-planar environment. Further work is planned in order to obtain electrochemically ions of $[Rh_2\{\mu\text{-}S(CH_2)_nS\}(cod)_2]$ and $[Rh_2\{\mu\text{-}S(CH_2)_nS\}(CO)_4]$. Their chemistry could be quite different to that of their neutral partners.

Laplacian of Charge Density.—Fig. 3(*a*) shows contour maps of the laplacian of the charge density ($\nabla^2\rho$) in a plane containing a Rh and the two S atoms. Dashed contours are used for negative values of $\nabla^2\rho$, whereas solid lines are for 0 and positive values of $\nabla^2\rho$. As in the complexes $[Rh_2\{NC(S)(CH_2)_3\}_4]$ and $[Rh_2\{NC(S)(CH_2)_3\}_4(CO)]$ the rhodium atom exhibits only four shells of charge concentration. The fourth shell should be referred as the inner valence shell of charge concentration (i.v.s.c.c.).[23,48] The i.v.s.c.c. is highly polarized by the presence of the ligands. In the square-planar geometry the metal atom exhibits six maxima of charge concentration. Four of these have values of −16.0 au and are on the RhS_2 plane, and two are on the perpendicular plane with magnitudes of −11.7 au (see schematic representation in Fig. 4).

In terms of the laplacian of charge density a co-ordinative M–L bond is characterized by two critical points on the M–L line, a maximum of charge concentration in the valence shell of the ligand and a maximum of charge depletion in the valence shell of the metal, that is a minimum in the $\nabla^2\rho$ function.[27,28]

The number and distribution of the (3,−3) critical points on the i.v.s.c.c. of a metal atom in an organometallic system depends mainly on the ligand distribution and less on the number of electrons in the metal valence shell. For instance, the rhodium atoms in the Rh_2^{4+} complexes[49] are formally Rh^{II}. In dinuclear rhodium complexes with thiocaprolactamate ligands the rhodium atoms present net charges between +0.38 and +1.08e.[49] Although in these rhodium(II) complexes the electron densities of the rhodium atoms are smaller than in the present dithiolate complex (0.05 e is the net charge associated with each metal centre) the rhodium atoms exhibit eight charge concentrations. They are imposed by the presence of the four equatorial ligands and the axial M–M and M–CO interaction.[27] Eight charge concentrations is also the number of maxima on the i.v.s.c.c. of an atom in an octahedral environment.[48]

Fig. 3(*b*) shows the contour maps of $\nabla^2\rho$ in a plane containing the two metal atoms and perpendicular to the SCH_2CH_2S ligand. Although in this plane the Rh atoms also exhibit four maxima in the i.v.s.c.c., this shell presents a lower polarization than in the RhS_2 plane [Fig. 3(*a*)]. This is clearly due to the absence of ligands in this plane. Fig. 3(*c*) displays contour maps of the laplacian of density in the plane of the bridging ligand. The sulfur atom presents two maxima in $\nabla^2\rho$ in the plane containing the dithiolate ligand, one of bonded type in the direction of the carbon atom and one of non-bonded type, both forming an angle of 109.2° (see Fig. 4). The relative values are respectively −0.251 and −0.473 au. The two other maxima of the sulfur atoms are directed towards each rhodium centre. They represent the electron-pair donation of the sulfur atoms to the metals. The electronic charge of the bridging ligand is only −0.58 e, the charges associated with the S and C atoms being −0.33 and −0.40 e respectively.

The substitution of cods by CO groups alters somewhat the electron distribution of the Rh atoms. The most significant change is the transformation of the two maxima, located in the plane perpendicular to the square planar plane, into two (3,−1) critical points. The values of $\nabla^2\rho$ at the critical points are −11.7 au for complex **1** and −9 au for **3**, respectively. This is a consequence of the important π-acceptor character of the CO ligand.

Experimental

All syntheses of rhodium complexes were performed using standard Schlenk techniques under a nitrogen atmosphere. Solvents were distilled and deoxygenated before use. All other reagents were used as commercially supplied. The complex $[\{Rh(\mu\text{-}OMe)(cod)\}_2]$ was prepared as previously reported.[50] The C, H and S analyses were carried out using a Perkin Elmer 240B and a Carlo-Erba microanalyser. Conductivities were measured in *ca.* 2×10^{-4} mol dm^{-3} acetone solutions with a Philips PW-9509 conductimeter. The IR spectra (KBr pellets or dichloromethane solutions) were recorded on a Nicolet 5ZDX-FT instrument, ^1H and ^{13}C NMR spectra on a Varian Gemini 300 MHz spectrometer and referenced in the standard way.

Preparations.—$[Rh_2\{\mu\text{-}S(CH_2)_2S\}(cod)_2]$ **1**. The ligand $HS(CH_2)_2SH$ (11 μl, 0.13 mmol) was added to a solution of $[\{Rh(\mu\text{-}OMe)(cod)\}_2]$ (60 mg, 0.12 mmol) in dichloromethane. The yellow solution became orange. After stirring at room temperature for 10 min, diethyl ether was added to give a red precipitate which was filtered off and dried *in vacuo* (53 mg, 83% yield) (Found: C, 41.7; H, 5.4; S, 12.2. Calc. for $C_{18}H_{28}Rh_2S_2$: C, 42.0; H, 5.4; S, 12.4%). NMR ($CDCl_3$): ^1H, δ 4.6, 4.3 (t, CH=, cod), 2.6 (m, CH_2, ligand) and 2.1, 1.9 (m, CH_2, cod); $^{13}C\text{-}\{^1H\}$, δ 31.7, 31.9 (CH_2, cod), 33.9 (CH_2, ligand), 80.1 [d, CH=, cod, ^1J(RhC) = 11.2] and 80.9 [d, CH=, cod, ^1J(RhC) = 12.2 Hz]. Recrystallization from CH_2Cl_2–Et_2O gave suitable crystals for X-ray diffraction.

$[\{Rh_2[\mu\text{-}S(CH_2)_3S](cod)_2\}_n]$ (*n* = **22** *or* **13**). To a solution of $[\{Rh(\mu\text{-}OMe)(cod)\}_2]$ (60 mg, 0.12 mmol) in dichloromethane was added $HS(CH_2)_3SH$ (13 μl, 0.13 mmol) and after stirring at room temperature for 10 min the yellow solution became red. Addition of diethyl ether resulted in the precipitation of a yellow complex $[\{Rh_2[\mu\text{-}S(CH_2)_3S](cod)_2\}_2]$ **2** which was filtered off and dried *in vacuo* (15.8 mg, 12% yield). NMR ($CDCl_3$): ^1H, δ 4.1 (m, CH, cod), (2.4, br, CH_2, cod) 2.1 [t, SCH_2, ^3J(HH) = 5.3], 1.9 [d, ^2J(HH) = 7.9, CH_2, cod] and 1.7 [t, SCH_2CH_2, ^3J(HH) = 6.0 Hz]; $^{13}C\text{-}\{^1H\}$, δ 24.2 (SCH_2), 30.9 (s, CH_2, cod) and 78.6 [d, CH, cod, ^1J(RhC) = 13.9 Hz]. After the separation of the yellow complex the solvent of the resulting solution was evaporated under reduced pressure to 2 cm^3. After cooling the flask in ice a red product $[Rh_2\{\mu\text{-}S(CH_2)_3S\}(cod)_2]$ **3** was obtained, filtered off, washed with methanol and vacuum dried (14 mg, 22% yield). Recrystallization at −20 °C from a saturated solution gave red crystals (Found: C, 43.2; H, 5.7; S, 11.30. Calc. for $C_{19}H_{30}Rh_2S_2$: C, 43.2; H, 5.7; S, 12.1%). ^1H NMR ($CDCl_3$): δ 4.6, 4.3 (m, CH, cod), 2.5, 2.1 (m, CH_2, cod).

$[\{Ru_2[\mu\text{-}S(CH_2)_4S](cod)_2\}_n]$ **4**. The ligand $HS(CH_2)_4SH$ (25 μl, 0.1 mmol) was added to a solution of $[\{Rh(\mu\text{-}OMe)(cod)\}_2]$ (100 mg, 0.21 mmol) in dichloromethane. After stirring at room temperature for 10 min diethyl ether was added to give a yellow precipitate which was filtered off and dried *in vacuo* (94.3 mg, 84% yield) (Found: C, 43.4; H, 5.70; S, 11.5. Calc. for $C_{20}H_{32}Rh_2S_2$: C, 44.3; H, 5.9; S, 11.8%). ^1H NMR ($CDCl_3$); δ 4.1 (m, CH, cod), 2.4, 2.0 (m, CH_2, cod) and 2.0, 1.6 (m, CH_2).

$[Rh_2\{\mu\text{-}S(CH_2)_2S\}(CO)_4]$ **5**. Carbon monoxide was bubbled for 10 min through a solution of $[Rh_2\{\mu\text{-}S(CH_2)_2S\}(cod)_2]$ in dichloromethane. The initial red solution became dark. Addition of diethyl ether gave a black precipitate. It was filtered off, washed with diethyl ether and dried *in vacuo* (36.6 mg, 70% yield) (Found: C, 17.6; H, 0.9; S, 15.6. Calc. for $C_6H_4O_4Rh_2S_2$: C, 17.6; H, 1.0; S, 15.6%). IR (CH_2Cl_2, ν_{max}): 2085s, 2059s and 2019s cm^{-1}.

$[Rh_2\{\mu\text{-}S(CH_2)_3S\}(CO)_4]$ **6**. To a solution of $[\{Rh(\mu\text{-}OMe)(cod)\}_2]$ (60 mg, 0.12 mmol) in dichloromethane was added propane-1,3-dithiol (13 μl, 0.13 mmol). After 10 min of stirring, carbon monoxide was bubbled through the solution for 10 min. The yellow suspension became dark. On addition of methanol a dark red precipitate was formed. It was filtered off, washed with methanol and vacuum dried (39 mg, 74% yield) (Found: C, 19.3; H, 1.2; S, 15.8. Calc. for $C_7H_6O_4Rh_2S_2$: C, 19.8; H, 1.05; S, 15.1%). IR (CH_2Cl_2, ν_{max}): 2083s, 2061s and 2012s cm^{-1}.

$[Rh_2\{\mu\text{-}S(CH_2)_4S\}(CO)_4]$ **7**. Carbon monoxide was bubbled for 10 min through a solution of $[\{Rh_2[\mu\text{-}S(CH_2)_4S](cod)_2\}_2]$ (67.2 mg, 0.062 mmol) in dichloromethane (3 cm^3). The initial red solution became dark and a red precipitate was formed. It was filtered off, washed with diethyl ether and dried *in vacuo* (48.4 mg, 89% yield) (Found: C, 21.6; H, 1.7; S, 14.0. Calc. for $C_8H_8O_4Rh_2S_2$: C, 21.9; H, 1.8; S, 14.6%). IR (CH_2Cl_2, ν_{max}): 2075s, 2059s and 2007s cm^{-1}.

Structure of $[Rh_2\{\mu\text{-}S(CH_2)_2S\}(cod)_2]$ **1**.—*Crystal data.* $C_{18}H_{28}Rh_2S_2$, M = 514.4, monoclinic, space group $P2_1/m$, a = 6.863(2), b = 16.503(4), c = 7.949(4) Å, β = 99.78(4)°, U = 887.2 $Å^3$ (by least-squares fit of 25 reflections with 15 < 2θ < 21°, λ = 0.710 69 Å), Z = 2, D_c = 1.93 g cm^{-3}, $F(000)$ = 516. Red, parallelopipeds. Crystal dimensions 0.2 × 0.2 × 0.1 mm, μ(Mo-Kα) = 20.5 cm^{-1}.

Data collection and processing. CAD4 diffractometer, θ–2θ scan mode, scan mode Δθ = (0.8 + 0.35 tanθ)°, maximum scan time 1 min, graphite-monochromated Mo-Kα radiation. 1630 Measured unique reflections with 2 < θ < 25°, *h* 0–8, *k* 0–19, *l* −9 to 9. 1319 Observed reflections with $|F^2| > 3\sigma(F^2)$ where $\sigma(F^2) = [\sigma^2(I) + (0.04I)^2]^{\frac{1}{2}}/L_p$. Correction for Lorentz and polarization effects and for absorption (DIFABS);[51] maximum and minimum values 1.14 and 0.90. Two standard reflections measured every hour showed no significant change.

Structure analysis and refinement. Routine heavy-atom methods, full-matrix least squares with non-hydrogen atoms anisotropic and hydrogen atom positions refined but U_{iso} fixed at 1.3 U_{eq} of the carbon atom. $w = 1/\sigma^2(F)$, $\Sigma w(|F_o| - |F_c|)^2$ minimized. Final $R = 0.025$, $R' = 0.034$. Programs from the SDP Plus package[52] run on a MicroVax computer. Atomic scattering factors taken from ref. 53.

Structure of $[Rh_2\{\mu\text{-}S(CH_2)_2S\}(cod)_2]$ **3**.—*Crystal data*. $C_{19}H_{30}Rh_2S_2$, $M = 528.4$, monoclinic, space group $P2_1/m$, $a = 7.018(1)$, $b = 17.038(6)$, $c = 8.012(18)$ Å, $\beta = 99.24(8)°$, $U = 887.2$ Å^3 (by least-squares fit of 20 reflections with $15 < 2\theta < 18°$, $\lambda = 0.7109$ Å), $Z = 2$, $D_c = 1.86$ g cm^{-3}, $F(000) = 532$. Red blocks. Crystal dimensions 0.3 × 0.3 × 0.1 mm, μ(Mo-Kα) = 19.3 cm^{-1}.

Data collection and processing. As for complex **1**, except the following. 1737 Measured unique reflections with $2 < \theta < 25°$, h 0–8, k 0–20, l −9 to 9. 1447 Observed reflections with $|F^2| > 3\sigma(F^2)$ where $\sigma(F^2) = [\sigma^2(I) + (0.04I)^2]^{\frac{1}{2}}/L_p$. Maximum and minimum corrections for absorption 1.15 and 0.90.

Structure analysis and refinement. Routine heavy-atom methods showed C(10) to be disordered across the mirror plane. Full-matrix least-squares refinement, non-hydrogen atoms anisotropic, hydrogen atoms for bridging ligand omitted, other hydrogen atoms at calculated positions with U_{iso} fixed at 1.3 U_{eq} for the parent carbon atom. $w = 1/\sigma^2(F)$, $\Sigma w(|F_o| - |F_c|)^2$ minimized. Final $R = 0.033$, $R' = 0.053$.

Additional material available from the Cambridge Crystallographic Data Centre comprises H-atom coordinates, thermal parameters and remaining bond lengths and angles.

Acknowledgements

We thank Comision Interministerial de Ciencia y Technologia) (CICYT) (projects PB 86-0092 and PB-88-0252). Some functions were computed with the CRAY-XMP of Construcciones Aeronauticas Sociedad Anonima through a grant of computer time from the CICYT. We thank the staff of the C.A.S.A. computer center for their co-operation. P. A. C. and C. C. thank Accion Integrada Hispano-Británica 3/88 and Ciba-Geigy for financial support. We are also much indebted to the Laboratoire of Chimique Quantique for providing a copy of the ASTERIX system of programs and to Professor Bader for a copy of the AIMPACK package. We thank Peter Knowles for useful discussions.

References

1 W. Hieber and K. Heinicke, *Z. Naturforsch., Teil B*, 1961, **16**, 554.
2 J. Cooke, M. Green and F. G. A. Stone, *J. Chem. Soc. A*, 1968, 170.
3 E. S. Bolton, R. Havlin and G. R. Knox, *J. Organomet. Chem.*, 1969, **18**, 153.
4 B. F. G. Johnson, J. Lewis and P. W. Robinson, *J. Chem. Soc. A*, 1969, 2693.
5 J. V. Kingston and G. R. Scollary, *J. Inorg. Nucl. Chem.*, 1971, **33**, 4373.
6 G. Palvi, A. ViziOrosz, L. Marko, F. Marcati and G. Bor, *J. Organomet. Chem.*, 1974, **86**, 295.
7 L. Vaska and J. Peone jun., *Chem. Commun.*, 1971, 418.
8 R. D. W. Kemmitt and G. D. Rimmer, *J. Inorg. Nucl. Chem.*, 1973, **35**, 3155.
9 R. Hill, B. A. Kelly, F. G. Kennedy, S. A. Knox and P. Woodward, *J. Chem. Soc., Chem. Commun.*, 1977, 434.
10 Ph. Kalck and R. Poilblanc, *Inorg. Chem.*, 1975, **14**, 2779.
11 J.-J. Bonnet, P. Kalck and R. Poilblanc, *Inorg. Chem.*, 1977, **16**, 1514.
12 R. Choukround, D. Gervais, J. Jaud, Ph. Kalck and F. Senocq, *Organometallics*, 1986, **5**, 67.
13 C. Claver, Ph. Kalck, M. Ridmy, A. Thorez, L. A. Oro, M. T. Pinillos, M. C. Apreda, F. H. Cano and C. Foces-Foces, *J. Chem. Soc., Dalton Trans.*, 1988, 1523.
14 D. Cruz-Garritz, B. Rodriguez, H. Torrens and J. Leal, *Transition Met. Chem.*, 1984, **9**, 284.
15 R. M. Catala, D. Cruz-Garritz, A. Hills, D. L. Hughes, R. L. Richards, P. Sosa, P. Terreros and H. Torrens, *J. Organomet. Chem.*, 1989, **359**, 219.
16 C. Claver, A. M. Masdeu, N. Ruiz, C. Foces-Foces, F. H. Cano, M. C. Apreda, L. A. Oro, J. Garcia-Alejandre and H. Torrens, *J. Organomet. Chem.*, 1990, **398**, 177 and refs. therein.
17 Ph. Kalck, J. M. Frances, P. M. Pfister, T. G. Southern and A. Thorez, *J. Chem. Soc., Chem. Commun.*, 1983, 510.
18 Ph. Kalck, in *Organometallics in Organic Syntheses*, eds. A. de Meijere and H. Tom Dick, Springer, Hamburg, 1987, pp. 297–320.
19 A. Polo, C. Claver, S. Castillón, A. Ruiz, J. C. Bayón, J. Real, C. Mealli and D. Masi, *Organometallics*, 1992, **11**, 3525; A. Polo, Ph.D. Thesis, Tarragona, 1990; A. Polo, E. Fernandez, C. Claver and S. Castillón, *J. Chem. Soc., Chem. Commun.*, 1992, 639.
20 J. C. Bayon, P. Esteban, J. Real, C. Claver and A. Ruiz, *J. Chem. Soc., Chem. Commun.*, 1989, 1056.
21 R. F. W. Bader, *Acc. Chem. Res.*, 1985, **18**, 9.
22 (*a*) R. F. W. Bader and H. Essem, *J. Chem. Phys.*, 1980, **80**, 1943; (*b*) R. F. W. Bader, P. J. MacDougall and C. D. H. Lau, *J. Am. Chem. Soc.*, 1987, **106**, 485.
23 R. F. W. Bader, R. J. Gillespie and P. J. Macdougall, *J. Am. Chem. Soc.*, 1988, **110**, 7329.
24 R. Ernenwein, M. Rohmer and M. Benard, *Comput. Phys. Commun.*, 1990, **58**, 305; M. M. Rohmer, J. Demuynck, M. Benard, R. Wiest, C. Bachmann and C. Henriet, *Comput. Phys. Commun.*, 1990, **60**, 127; R. Wiest, J. Demuynck, M. Benard, M. M. Rohmer and R. Ernenwein, *Comput. Phys. Commun.*, 1991, 62, 107.
25 A. Veillard and A. Dedieu, *Theor. Chim. Acta*, 1984, **65**, 215.
26 S. Huzinaga, Technical Report, University of Alberta, Edmonton, 1971.
27 C. Bo, J. M. Poblet and M. Benard, *Chem. Phys. Lett.*, 1990, **169**, 89.
28 M. Costas, C. Bo and J. M. Poblet, *Chem. Phys. Lett.*, 1992, **200**, 8.
29 A. A. Low, K. L. Kunze, P. J. MacDougall and M. B. Hall, *Inorg. Chem.*, 1991, **30**, 1079.
30 R. F. W. Bader, *Atoms in Molecules. A Quantum Theory*, Clarendon Press, Oxford, 1990.
31 F. W. Biegler-Konig, R. F. W. Bader and T. H. Tang, *J. Comput. Chem.*, 1982, **3**, 317.
32 J. J. Bonnet, A. Thorez, A. Maisonnat, J. Galy and R. Poilblanc, *J. Am. Chem. Soc.*, 1979, **101**, 5940.
33 L. F. Dahl, C. Martell and D. L. Wampler, *J. Am. Chem. Soc.*, 1961, **83**, 1761.
34 M. G. B. Drew, S. M. Nelson and M. Sloan, *J. Chem. Soc., Dalton Trans.*, 1973, 1484.
35 J. J. Bonnet, Y. Jeannin, Ph. Kalck, A. Maissonnat and R. Poilblanc, *Inorg. Chem.*, 1975, **14**, 743.
36 P. B. Hitchcock, S. Morton and J. F. Nixon, *J. Chem. Soc., Dalton Trans.*, 1985, 1295.
37 A. C. King, B.Sc. Thesis, University of Sussex, 1988.
38 K. A. Beveridge, G. W. Bushnell, S. R. Stobart, J. L. Atwood and M. J. Zaworotko, *Organometallics*, 1983, **2**, 1447.
39 L. A. Oro, M. T. Pinillos, C. Tejel, C. Foces-Foces and F. H. Cano, *J. Chem. Soc., Dalton Trans.*, 1986, 1087.
40 R. Usón, L. A. Oro, M. A. Ciriano, M. T. Pinillos, A. Tiripicchio and M. Tiripicchio, Camellini, *J. Organomet. Chem.*, 1981, **205**, 247.
41 R. Usón, L. A. Oro, M. A. Ciriano, D. Carmona, A. Tiripicchio and M. Tiripicchio Camellini, *J. Organomet. Chem.*, 1981, **206**, C14.
42 N. G. Connelly, G. A. Johnson, B. A. Kelly and P. Woodward, *J. Chem. Soc., Chem. Commun.*, 1977, 436.
43 A. M. Mueting, P. Boyle and L. H. Pignolet, *Inorg. Chem.*, 1984, **23**, 44.
44 M. Costas, T. Leininger, G. H. Jeung and M. Benard, *Inorg. Chem.*, 1992, **31**, 3317.
45 D. L. Lichtenberger, A. S. Copenhauer, H. B. Gray, J. L. Marshall and M. D. Hopkins, *Inorg. Chem.*, 1988, **27**, 4488.
46 S. K. Kang, T. A. Albright, T. C. Wright and R. A. Jones, *Organometallics*, 1985, **4**, 666; R. Summerville and R. Hoffmann, *J. Am. Chem. Soc.*, 1976, **98**, 7240.
47 See, for instance, *Quantum Chemistry. The Challenge of Transition Metals and Coordination Chemistry*, ed. A. Veillard, NATO ASI Series C, 1985, vol. 176.
48 C. Bo, J. P. Sarasa and J. M. Poblet, *J. Phys. Chem.*, in the press.
49 J. M. Poblet and M. Benard, *Inorg. Chem.*, 1988, **27**, 2935.
50 R. Usón, L. A. Oro and J. A. Cabeza, *Inorg. Synth.*, 1985, **23**, 126.
51 N. Walker and D. Stuart, DIFABS, program for empirical absorption corrections, *Acta Crystallogr., Sect. A*, 1968, **24**, 321.
52 SDP Plus, Structure Determination Package, Enraf-Nonius, Delft, 1982.
53 *International Tables for X-Ray Crystallography*, Kynoch Press, Birmingham, 1974, vol. 4.

Received 26*th January* 1993; *Paper* 3/00493G